American Mineralogist, Volume 94, pages 98–104, 2009

Lattice thermal expansion of zircon-type $LuPO_4$ and $LuVO_4$: A comparative study

S.J. Patwe, S.N. Achary,* and A.K. Tyagi†

Chemistry Division, Bhabha Atomic Research Centre, Mumbai 400085, India

Abstract

We report the lattice thermal expansion of zircon-(xenotime-)type $LuPO_4$ and $LuVO_4$ in the temperature range of 25–1000 °C from high-temperature powder XRD studies. The details of the high-temperature crystal chemistry of both phases have been determined from Rietveld analysis of the powder XRD data. Both the compounds show appreciably higher thermal expansion than analogous zircon-type silicates. Despite isomorphism, the axial thermal expansion of $LuVO_4$ shows significant anisotropy compared to $LuPO_4$. In the studied temperature range, the average axial thermal expansion coefficients of $LuPO_4$ are $\alpha_a = 6.0 \times 10^{-6}$ and $\alpha_c = 7.2 \times 10^{-6}$ ($°C^{-1}$) and those of $LuVO_4$ are $\alpha_a = 3.6 \times 10^{-6}$ and $\alpha_c = 11.8 \times 10^{-6}$ ($°C^{-1}$). However, the average volume thermal expansion coefficients are almost identical. The differences in the thermal expansion behavior of the two structures originate from differences in the expansion and distortion of the LuO_8 polyhedra. The LuO_8 polyhedron in $LuVO_4$ shows about 30% higher thermal expansion than that in $LuPO_4$. The overall thermal expansion behaviors of these two structures are predominantly related to the distortion in the LuO_8 unit, inter-cation distances and spatial arrangement of the Lu-O bonds in the structure.

Keywords: Thermal expansion, crystal chemistry, zircon, xenotime, phosphates, vanadates

Introduction

The ABO_4-type compounds have been of interest because of technologically important physical properties (Kaminskii 1990; Scott et al. 2002) as well as mineralogical importance in understanding their crystal chemistry (Knittle and Williams 1993). The diversity of crystal chemistry of ABO_4 compounds is controlled by the ionic radii and charge combination of the A and B cations (Carron et al. 1958; Aldred 1984; Depero and Sangalettis 1997; Muller and Roy 1974). Depending on the ionic radii and charge combination of the cations, these compounds crystallize in scheelite-, monazite-, zircon-, and wolframite-type structures. Among the ABO_4 compounds with A^{3+} and B^{5+} combinations, structures related to scheelite ($I4_1/a$), monazite ($P2_1/c$), zircon ($I4_1/amd$), $MnSO_4$ (*Cmcm*), $CrPO_4$ (*Imma*), and silica, are known either at ambient or non-ambient pressure-temperature conditions. However, with a rare earth, viz. La-Lu, Y, and Sc as one of the trivalent ions, the only crystal structures known for B = P and V cation are monazite- and zircon-type structures (Beall et al. 1981; Boatner 2002; Ni et al. 1995; Chakoumakos et al. 1994; Mullica et al. 1996). Almost all the heavier lanthanide phosphates and vanadates crystallize in zircon-type structures. The structural studies on these compounds under high pressure and/or high temperature revealed various displacive and reconstructive transformations in them (Errandonea et al. 2004; Jayaraman et al. 1985; Wang et al. 2004; Sen et al. 2003; Mittal et al. 2008).

The zircon-(xenotime-)type ABO_4 materials are known for their low thermal expansion and incompressible stable structure under moderate pressure. However, under significantly higher pressure, zircon and its analogs transform to scheelite and post-scheelite structures. Also, among the zircon-group materials the thermal expansion behaviors are drastically different depending upon the cation charge and ionic radii combination (Bayer 1972; Subbarao et al. 1990; Li et al. 2007; Taylor 1986). Although both phosphates and vanadates of rare-earth ions have similar structural arrangements of AO_8 (bisdisphenoid, A = trivalent rare-earth ion) and PO_4 or VO_4 tetrahedra (Ni et al. 1995; Chakoumakos et al. 1994; Mullica et al. 1996), the differences in thermophysical behaviors due to the tetrahedral groups are remarkable. To evaluate the effect of ionic radii on the thermal expansion of these materials, several high-temperature studies have been performed on rare-earth vanadates and phosphates (Bayer 1972; Subbarao et al. 1990; Li et al. 2007; Taylor 1986; N. Reddy et al. 1981; Reddy et al. 1985, 1988, 1995). A comparison of the thermal expansion behavior of various zircon-group compounds shows significantly more anisotropic expansion for vanadates than phosphates. In addition, among these zircon-type ABO_4 compounds, heavier rare-earth phosphates and vanadates show significant anisotropy (Bayer 1972; Subbarao et al. 1990; Li et al. 2007; Taylor 1986). However, the detailed variations of the crystal structure or role of the crystal structures responsible for this have not been explained. It is well known that the increase in the mean bond length due to increasing amplitude of vibration of the atoms with temperature is reflected in the expansion of the material. Often crystal structure provides an explanation for thermal expansion behavior of a material. There are several reports correlating thermal expansion behavior with structural arrangements available in the literature (Khan 1976; Evans et al. 1996;

* E-mail: sachary@barc.gov.in
† E-mail: aktyagi@barc.gov.in

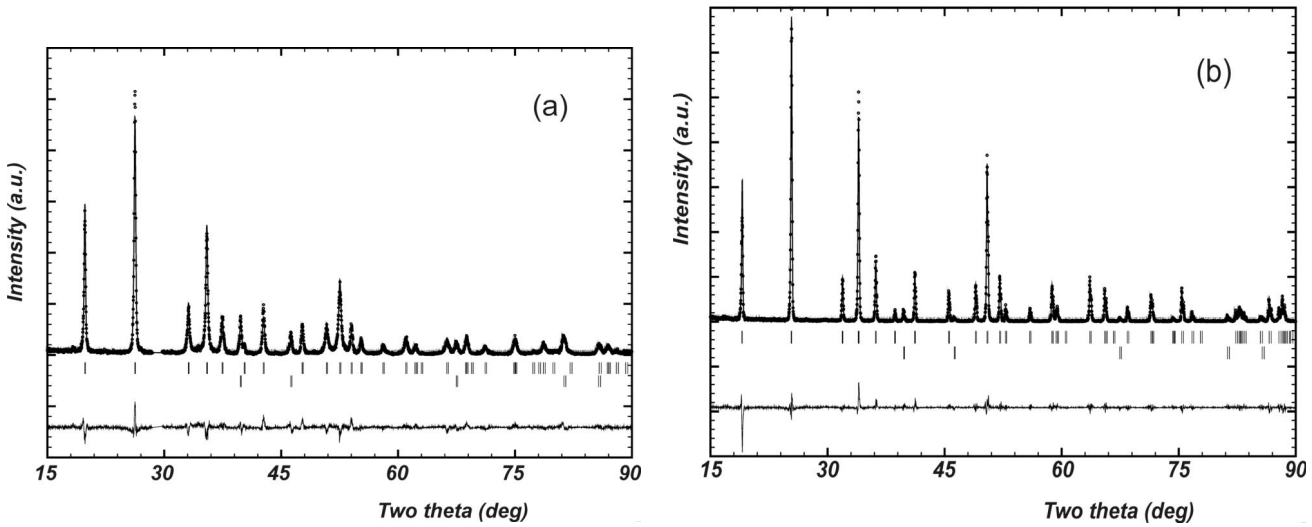

FIGURE 1. Rietveld refinement plot of (**a**) $LuPO_4$ and (**b**) $LuVO_4$ at 25 °C. The vertical lines below the diffraction profile indicate Bragg positions (upper) for sample and (lower) for platinum.

Achary et al. 2003; Achary and Tyagi 2004; Haines et al. 2004; Varga et al. 2005; Gates et al. 2006). To compare the structural differences due to the PO_4 and VO_4 group in a particular structure and its effect on thermal expansion, detailed high-temperature, crystal-structure analyses of these two title compounds are carried out, and the results are presented in this paper.

EXPERIMENTAL METHODS

$LuVO_4$ was prepared by heating appropriate amounts of Lu_2O_3 and V_2O_5 (AR grade) at 800 °C for 12 h followed by a re-homogenization and reheating at 1100 °C for 8 h. $LuPO_4$ was prepared by heating appropriate amounts of Lu_2O_3 and $(NH_4)_2HPO_4$ at 300 °C for the decomposition of $(NH_4)_2HPO_4$. The decomposed product obtained was reground, pelletized, and heated at 900 and 1100 °C (for 12 h at each temperature). The final products were checked by powder XRD on a Philips PW1710 model powder X-ray diffractometer for phase purity. The XRD patterns of the samples at various temperatures were collected in air on a Philips X-Pert Pro diffractometer. The XRD patterns were recorded in the 2θ range 15–90° with step width and step time of 0.02° and 1.25 s, respectively. The sample was heated to a desired temperature at the rate of 20 °C/min and held for 5 min for equilibration and then XRD data were collected. The Rietveld refinements of the powder diffraction profiles were carried out using Fullprof (Rodriguez-Caravajal 1990).

RESULTS AND DISCUSSION

The phase purity of the $LuPO_4$ and $LuVO_4$ samples was confirmed from the powder XRD patterns by comparing them with previously published diffraction data. However, in the $LuPO_4$ sample, weak additional reflections observed at 29.3 and 30.1 °2θ [d and I/I_0 are 2.96 Å (2.6%) and 3.05 Å (2.9%)] were assigned to $Lu_{12}P_2O_{23}$ (PDF 34-1444). The formation of this phase is due to either phosphorous deficiency in the initial mixture or high-temperature decomposition of $LuPO_4$. Since no structural details for this phase are available, the extra reflections were excluded from the analyses of the XRD patterns. Detailed analyses were carried out by Rietveld refinement of the powder XRD data for $LuVO_4$ and $LuPO_4$. The starting models for the refinement of room-temperature data were taken from the reported crystal structures (Ni et al. 1995; Chakoumakos et al. 1994; Mullica et al. 1996). All the diffraction patterns were subjected to two-phase refinements to accommodate additional reflections that appeared from the platinum sample holder. Initially, the scale, background, and unit-cell parameters were refined for both phases. Pseudo-Voigt profile functions were used to fit the peak profiles of both sample and platinum. The half-width, mixing parameters, preferred orientation, and asymmetry parameters were also refined. Subsequently, the atomic coordinates of O atoms and thermal parameters of all atoms were refined. The Rietveld refinement plots for the ambient-temperature data for both the samples are shown in Figures 1a and 1b. The details of the refined parameters for $LuVO_4$ and $LuPO_4$ are given in Tables 1 and 2, and are found to be consistent with previously reported data (Ni et al. 1995; Chakoumakos et al. 1994; Mullica et al. 1996).

$LuPO_4$ and $LuVO_4$ crystallize as xenotime structures that are made up of chains formed by alternating AO_8 polyhedra (bisdisphenoid) and BO_4 (tetrahedra) along the c-axis. These chains are joined together by sharing other edges of the AO_8 polyhedra along the a- and b-directions to form a three-dimensional lattice. A three-dimensional representation of the xenotime-type ABO_4 structure is shown in Figure 2a. A chain of alternating AO_8 and BO_4 polyhedra is shown in Figure 2b. The three-dimensional arrangement shows a close similarity to the rutile structure except for the anion distribution that leads to the eight- and four-coordinated polyhedra in the xenotime structure instead of the six- and six-coordinated cation polyhedra of the rutile structure. The polyhedral relations in the ABO_4-type compounds have been reported in the literature (Nyman and Hyde 1984). In both cases, the anions are bonded to three cations. The refined crystallographic parameters, P-O or V-O and Lu-O bond lengths at ambient temperature are in agreement with the values reported previously in the literature (Ni et al. 1995; Chakoumakos et al. 1994; Mullica et al. 1996).

The connection of LuO_8 units as well as LuO_8 and BO_4 units in the xenotime-type structure are shown in Figures 3a and 3b. There are four neighboring Lu and four neighboring B atoms to each Lu atom at the same distance (Table 3). Along the c axis, there are two additional B atoms with shorter Lu-B distances than the other four B atoms. The LuO_8 polyhedra made up of

TABLE 1. Crystallographic parameters of $LuVO_4$ at various temperatures

T (°C)	*a* (Å)*	*c* (Å)†	*V* (Å³)‡	B (Lu) (Å²)	B (V) (Å²)	Oxygen position coordinates		
						y	*z*	B (Å²)
25	7.0230(1)	6.2305(1)	307.31(1)	0.53(4)	0.16(10)	0.4362(8)	0.2039(10)	0.8(2)
100	7.0242(1)	6.2355(1)	307.66(1)	0.46(4)	0.17(10)	0.4360(8)	0.2032(10)	0.9(2)
200	7.0265(1)	6.2423(1)	308.19(1)	0.58(4)	0.26(10)	0.4368(8)	0.2050(10)	1.2(2)
300	7.0288(1)	6.2494(1)	308.74(1)	0.66(4)	0.31(10)	0.4363(9)	0.2053(10)	1.6(2)
400	7.0313(1)	6.2570(1)	309.34(1)	0.83(5)	0.53(11)	0.4374(9)	0.2068(11)	1.9(2)
500	7.0340(1)	6.2643(1)	309.94(1)	1.05(5)	0.68(11)	0.4373(9)	0.2076(11)	2.1(2)
600	7.0367(1)	6.2718(1)	310.55(1)	1.19(5)	0.62(11)	0.4352(9)	0.2051(11)	2.2(2)
700	7.0395(1)	6.2796(2)	311.18(1)	1.36(0)	0.86(12)	0.4361(10)	0.2066(11)	2.8(3)
800	7.0422(1)	6.2873(2)	311.80(1)	1.47(5)	0.89(12)	0.4369(10)	0.2083(12)	2.9(3)
900	7.0454(1)	6.2951(2)	312.47(1)	1.65(6)	1.34(13)	0.4379(10)	0.2088(12)	3.0(3)
1000	7.0478(1)	6.3022(2)	313.04(1)	1.74(6)	1.18(13)	0.4382(11)	0.2100(13)	3.4(3)

Notes: Space group $I4_1/amd$, no. 141, $Z = 4$, Lu (4*a*: 0, 3/4, 1/8), V (4*b*: 0, 1/4, 3/8), O (16*h*: 0, *y*, *z*).
Linear fit functions for unit-cell parameters (in the range of 25–1000 °C):
* a (Å) = 7.0214(3) + 2.60(5) × 10^{-5} (T)
† c (Å) = 6.2277(3) + 7.42(5) × 10^{-5} (T)
‡ V (Å³) = 307.02(4) + 0.0060(7) × (T)
where T = temperature in °C.

TABLE 2. Crystallographic parameters of $LuPO_4$ at various temperatures

T (°C)	*a* (Å)*	*c* (Å)†	*V* (Å³)‡	B (Lu) (Å²)	B (P) (Å²)	Oxygen position coordinates		
						y	z	B (Å²)
25	6.7895(3)	5.9560(4)	274.56(2)	0.48(7)	1.5(2)	0.4277(10)	0.2163(12)	1.0(3)
100	6.7914(3)	5.9585(4)	274.82(2)	0.61(7)	1.6(2)	0.4275(10)	0.2160(12)	1.4(3)
200	6.7951(4)	5.9618(5)	275.28(3)	0.36(11)	1.7(2)	0.4268(11)	0.2157(14)	1.4(3)
300	6.7989(3)	5.9664(4)	275.80(3)	0.86(7)	1.6(2)	0.4285(10)	0.2182(12)	1.4(3)
400	6.8050(3)	5.9725(4))	276.58(3)	0.84(7)	1.6(2)	0.4275(10)	0.2174(12)	1.6(3)
500	6.8090(3)	5.9768(4)	277.10(3)	1.00(8)	1.9(3)	0.4285(10)	0.2193(12)	1.8(3)
600	6.8132(3)	5.9814(4)	277.65(3)	1.08(8)	1.8(3)	0.4272(11)	0.2175(13)	2.2(3)
700	6.8171(4)	5.9859(4)	278.18(3)	1.11(8)	2.1(3)	0.4277(11)	0.2185(13)	2.3(3)
800	6.8214(4)	5.9893(4)	278.69(3)	1.33(8)	2.5(3)	0.4268(11)	0.2175(13)	2.4(3)
900	6.8249(4)	5.9932(4)	279.16(3)	1.33(8)	2.6(3)	0.4260(11)	0.2167(13)	2.7(3)
1000	6.8295(3)	5.9981(4)	279.76(3)	1.46(9)	2.4(3)	0.4268(11)	0.2181(13)	2.4(3)

Notes: Space group $I4_1/amd$, no. 141, $Z = 4$, Lu (4*a*: 0, 3/4, 1/8), P (4*b*: 0, 1/4, 3/8), O (16*h*: 0, y, z).
Linear fit functions for unit-cell parameters (in the range of 25–1000 °C):
* a (Å) = 6.7875(4) + 4.21(7) × 10^{-5} (T)
† c (Å) = 5.9542(4) + 4.41(8) × 10^{-5} (T)
‡ V (Å³) = 274.30(5) + 0.0055(9) × (T)
where T = temperature in °C.

two sets of four identical Lu-O bonds can be described as two interpenetrating tetrahedra. The set of four longer bonds (Lu-O_c) forms a tetrahedron elongated along the *c* axis. Similarly, the set of four shorter bonds (Lu-O_a) is compressed along the *c* axis and thus oriented more toward the *a* or *b* directions. The elongated tetrahedra formed with O_c atoms and compressed tetrahedra formed by the O_a atoms surrounding the Lu are shown in Figure 3. The values of Lu-O_a and Lu-O_c bonds at ambient temperature are given in Table 3.

The significant difference in the Lu-O bond lengths in these two structures due to the change in B cation from V to P is reflected in all the differences in the crystal structure and hence all the derived properties. In addition, the distortion and volume of the LuO_8 unit in $LuVO_4$ is larger than that in $LuPO_4$, which is reflected in the larger unit-cell parameters, volume, and larger *c/a* ratio of the vanadate (Table 4). The larger tetrahedral volume in $LuVO_4$ compared to $LuPO_4$ is expected from the larger ionic radius of V^{5+} compared to P^{5+}.

All the XRD patterns recorded at other temperatures were refined by the Rietveld method using the model structure based on the refined ambient-temperature structures. These XRD patterns appear similar to their corresponding ambient-temperature patterns. The refinements of the high-temperature XRD patterns of $LuVO_4$ and $LuPO_4$ were carried out in a procedure similar to that followed for ambient-temperature patterns. The refined unit-cell parameters and structural parameters for $LuVO_4$ and $LuPO_4$ at various temperatures are given in Tables 1 and 2. A smooth expansion in the unit-cell parameters with temperature is observed for both compounds.

The thermal expansion coefficients and axial ratios of the $LuPO_4$ and $LuVO_4$ are summarized in Table 4. From Table 4, it can be concluded that the *c* axis in $LuVO_4$ shows significantly higher thermal expansion than the *a* axis. However, almost identical expansions along the *a* and *c* axes are observed for $LuPO_4$. The difference in anisotropy of thermal expansion of $LuVO_4$ compared to $LuPO_4$ can be directly visualized from the variation of the *c/a* ratio with temperature (Fig. 4 and Table 4). However, the average coefficients of volume and linear [i.e., $1/3(\alpha_a + \alpha_a + \alpha_c)$] thermal expansion for $LuPO_4$ and $LuVO_4$ are more or less identical.

A comparison of the thermal expansion coefficients of $LuPO_4$ and $LuVO_4$ from this study with previously reported values for various isostructural phosphates and vanadates shows a close similarity, within the experimental errors (Table 5). The average linear expansion of $LuPO_4$ observed in the present study is marginally higher than the values reported for YPO_4, $ErPO_4$, $YbPO_4$, and $LuPO_4$ from dilatometric studies of sintered pellets (Hikishi et al. 1998). However, the present value of α_{av} is significantly higher than the values reported for other phosphates, namely, YPO_4 (Bayer 1972) and $ScPO_4$ (Subbarao et al. 1990; Taylor

1986). Recent theoretically calculated thermal expansion coefficients for the analogous phosphates (6.7 to 6.9 × 10^{-6} °C^{-1}) (Li et al. 2007) are higher than the present observed values. Similarly, the observed values of axial thermal expansion coefficients of $LuVO_4$ are comparable to the values reported for various other rare-earth vanadates (Table 5). The lower values of thermal expansion coefficients in the studies of Reddy et al. (1985, 1988), Zhao et al. (2004), and Skanthakumar et al. (1995) may be due to the difference in the temperature range of the studies. Compared to all other vanadates, $ScVO_4$ shows the largest anisotropy (Subbarao et al. 1990; Kahle et al. 1970; Schopper et al. 1972). Thus, the thermal expansion quadratic of rare-earth vanadates is an ellipsoid with elongation along the *c* axis. The thermal expansion behavior of $EuVO_4$ has an anomalous trend compared to other rare-earth vanadates (Reddy and Murthy 1983).

To understand the thermal expansion and possible effect of the crystal structure, variations of crystallographic, and derived structural parameters with temperature were analyzed. A comparison of variation of interatomic distances shows that the V-O or P-O bonds do not change significantly with temperature, which may be attributed to the strong bonding interaction leading to rigid polyhedra. However, all other bonds in both the compounds expand significantly with increase in temperature. The interatomic distances of selected bonds at 1000 °C are included in Table 3, as are the thermal expansion coefficients and the fitting functions for various interatomic distances. The polyhedral

TABLE 3. Selected interatomic distances and polyhedral parameters of LuO_8 units of $LuPO_4$ and $LuVO_4$ at 25 and 1000 °C

	$LuVO_4$				$LuPO_4$			
	T (°C)		α*	Linear fit (*T* in °C)†	*T* (°C)		α*	Linear Fit (*T* in °C)†
	25	1000			25	1000		
Lu-O_a ×4	2.262(8)	2.262(8)	3.4	2.258(2) + 0.8(4) × 10^{-5} (*T*)	2.255(7)	2.277(8)	10.8	2.253(2) + 2.4(3) × 10^{-5} (*T*)
S‡	0.46	0.456			0.469	0.438		
<λ>	1.511	1.437			1.422	1.408		
σ^2	1048	955			935	916		
Lu-O_c ×4	2.431(5)	2.493(8)	24.7	2.427(5) + 6.9(8) × 10^{-5} (*T*)	2.364(6)	2.386(7)	8.9	2.253(2) + 2.4(3) × 10^{-5} (*T*)
S‡	0.289	0.244			0.346	0.326		
<λ>	1.355	1.371			1.435	1.448		
σ^2	1321	1372			1562	1601		
V_{LuO_8} (Å^3)	23.04(10)	23.88(10)	38	22.98(2) + 8.8(4) × 10^{-4} (*T*)	22.05(10)	22.66(10)	29	2.9771(2) + 2.21(4) × 10^{-5} (*T*)
D§	13.6 ×10^{-4}	23.7 ×10^{-4}			5.6 ×10^{-4}	5.5 ×10^{-4}		
Lu-Lu (×4), Lu-B (×4)‖	3.8415(1)	3.8601(1)	5.1	3.8405(2) + 1.94(3) × 10^{-5} (*T*)	3.7070(1)	3.7295(1)	6.4	3.7058(2) + 2.37(4) × 10^{-5} (*T*)
Lu-B (×2)	3.1152(1)	3.1511(1)	11.9	3.1139(2) + 3.71(3) × 10^{-5} (*T*)	2.9780(1)	2.9990(1)	7.4	22.03(3) + 6.4(4) × 10^{-4} (*T*)

* Thermal expansion coefficient × 10^6 °C^{-1}.
† Linear fit functions to distances and volumes over the temperature range 25–1000 °C.
‡ S = Bond valence.
§ D = Distortion in LuO_8 units.
‖ The Lu-Lu and Lu-B distances are identical.

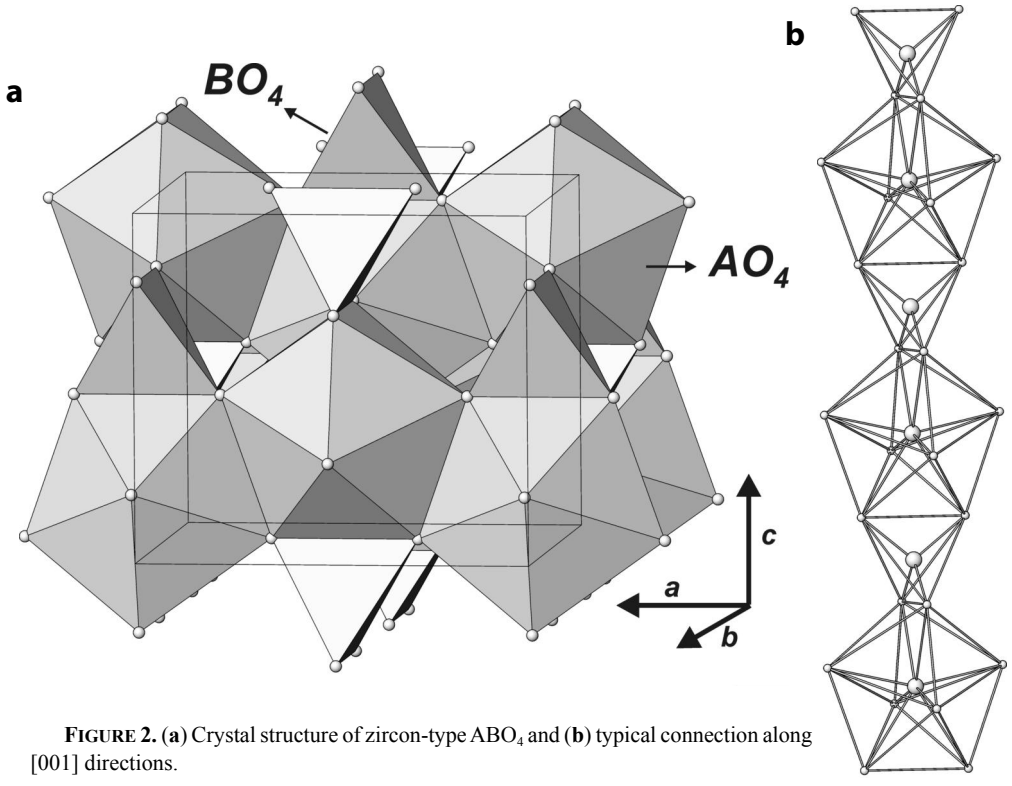

FIGURE 2. (**a**) Crystal structure of zircon-type ABO_4 and (**b**) typical connection along [001] directions.

units that are incompressible or show small compressibility are commonly observed in various oxides with higher positively charged cations as central ion. This has been explained on the basis of higher strength of cation-anion bonds (Hazen and Prewitt 1977). The higher bulk moduli and lower coefficients of thermal expansion have been observed for PO_4, VO_4, and SiO_4 tetrahedral units. The differences in the thermal expansion of Lu-O_a and Lu-O_c can be explained from the differences in the bond lengths and the arrangement of Lu-O bonds along the *a* and *c* axes. In particular, the orientation of the Lu-O bonds along the *a* and *c* axes and the variation of the O-Lu-O bond angles with temperature are predominantly related to the difference in the axial thermal expansions. Besides, the expansion of the Lu-O_c bonds significantly reduces the repulsive Lu-V interaction along the *c* axis. Thus, the thermal expansion coefficients of Lu-V bonds along the *c* axis are larger than those along *a* and *b* directions. Thus, the thermal expansion is always higher along the *c* axis in xenotime-type compounds. The significant differences in the thermal expansion behaviors of these bonds are related to the strongly anisotropic thermal expansion of $LuVO_4$ compared to $LuPO_4$.

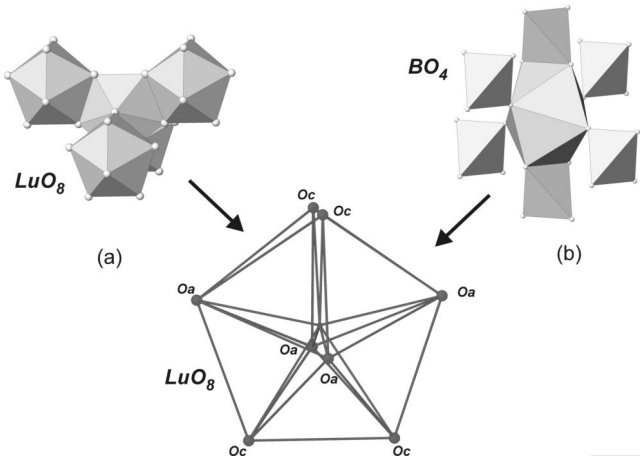

FIGURE 3. Typical polyhedral fragments (**a**) connections of LuO_8 units and (**b**) connections of BO_4 with LuO_8 in $LuPO_4$ or $LuVO_4$

TABLE 4. Thermal expansion coefficients and axial ratios of $LuPO_4$ and $LuVO_4$

	T (°C)	$LuPO_4$	$LuVO_4$
α_a (°C^{-1})	25–1000	6.04×10^{-6}	3.62×10^{-6}
α_c (°C^{-1})	25–1000	7.25×10^{-6}	11.80×10^{-6}
α_{av} (°C^{-1})*	25–1000	6.44×10^{-6}	6.34×10^{-6}
α_{vol} (°C^{-1})	25–1000	19.4×10^{-6}	19.1×10^{-6}
c/a	25	0.877	0.887
c/a	1000	0.878	0.894

* $\alpha_{av} = 1/3\ (\alpha_a + \alpha_a + \alpha_c)$.

TABLE 5. Comparison of thermal expansion data for relevant rare-earth phosphates and vanadates

	T range (°C)	α_{av} ($\times 10^{-6}$)	α_a ($\times 10^{-6}$)	α_c ($\times 10^{-6}$)	Reference
***APO*$_4$**					
Lu	25–1000	6.44	6.04	7.25	This work
Lu	20–1000	6.2			Hikishi et al. (1998)*
Er	20–1000	6.0			"
Yb	20–1000	6.0			"
Y	20–1000	6.2			"
Y	20–520		5.0	5.9	Bayer (1972)
Y	20–1020		5.4	6.0	"
Y	25–1000	5.7	–	–	Taylor (1986)*
Sc	20–1200	5.5	4.1	8.4	Subbarao et al. (1990)
***AVO*$_4$**					
Y	20–520		3.7	10.1	Bayer (1972)
Y	20–1020		4.0	10.5	"
Sc	20–1200		4.05	12.95	Schopper et al. (1972)
Sc	20–1200		3.9	14.	Kahle et al. (1970)
Y	27–670		3.1	7.21	Reddy et al. (1988)
Gd	25–540		2.16	8.92	Reddy et al. (1985)
Gd	25–1000		3.6	10.8	Anitha et al. (pers. comm.)
Gd	25–600		2.97	9.97	Anitha et al. (pers. comm.)
Nd	20–520		3.7	10.1	Bayer (1972)
Y	20–1020		4.0	10.5	"
$Lu_{0.95}Nd_{0.05}$	50–300		1.6	9.1	Zhao et al. (2004)
Lu	25–1000	6.34	3.62	11.80	This work
Lu	12–300 K		0.7	5.6	Skanthakumar et al. (1995)
Eu	27–670	–	8.72	3.24	Reddy and Murthy (1983)

Note: α_{av} is the linear thermal coefficient of expansion, and α_a and α_c are the thermal coefficients of expansion along *a* and *c*, respectively.
* Dilatometer on sintered pellets.

The distortions in the elongated $[Lu(O_c)_4]$ and compressed $[Lu(O_a)_4]$ tetrahedra (Fig. 3) are obviously reflected in the mean quadratic elongations ($\langle\lambda\rangle$) and bond angle variances (σ^2) (Robinson et al. 1971). The mean quadratic elongation and bond angle variances are calculated using the following equations:

$$\langle\lambda\rangle = \sum_{i=1}^{n} \left(\frac{li}{l_0}\right)^2 \Big/ n$$

$$\sigma^2 = \sum_{i=1}^{n} (\theta_i - \theta_0)^2 \Big/ (n-1)$$

where l_i and θ_i are observed bond lengths and bond angles:

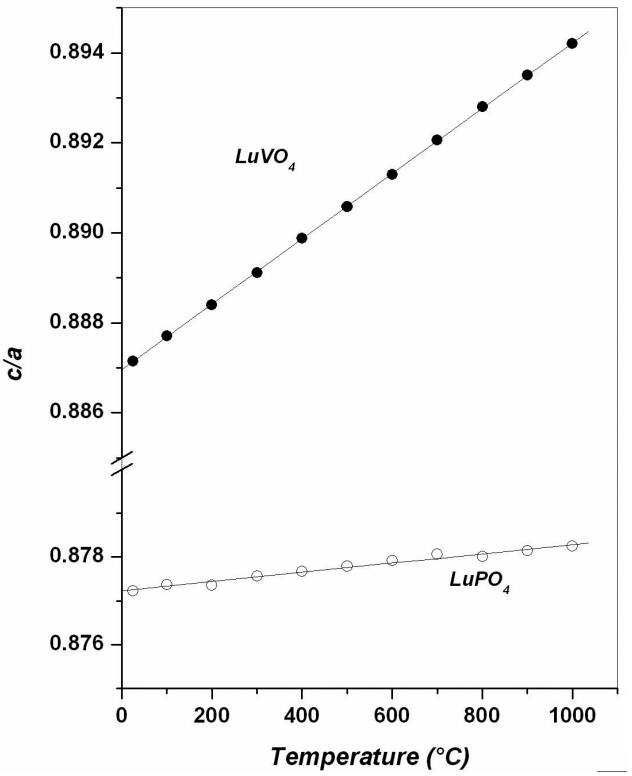

FIGURE 4. Variation of *c/a* of $LuPO_4$ and $LuVO_4$ with temperature.

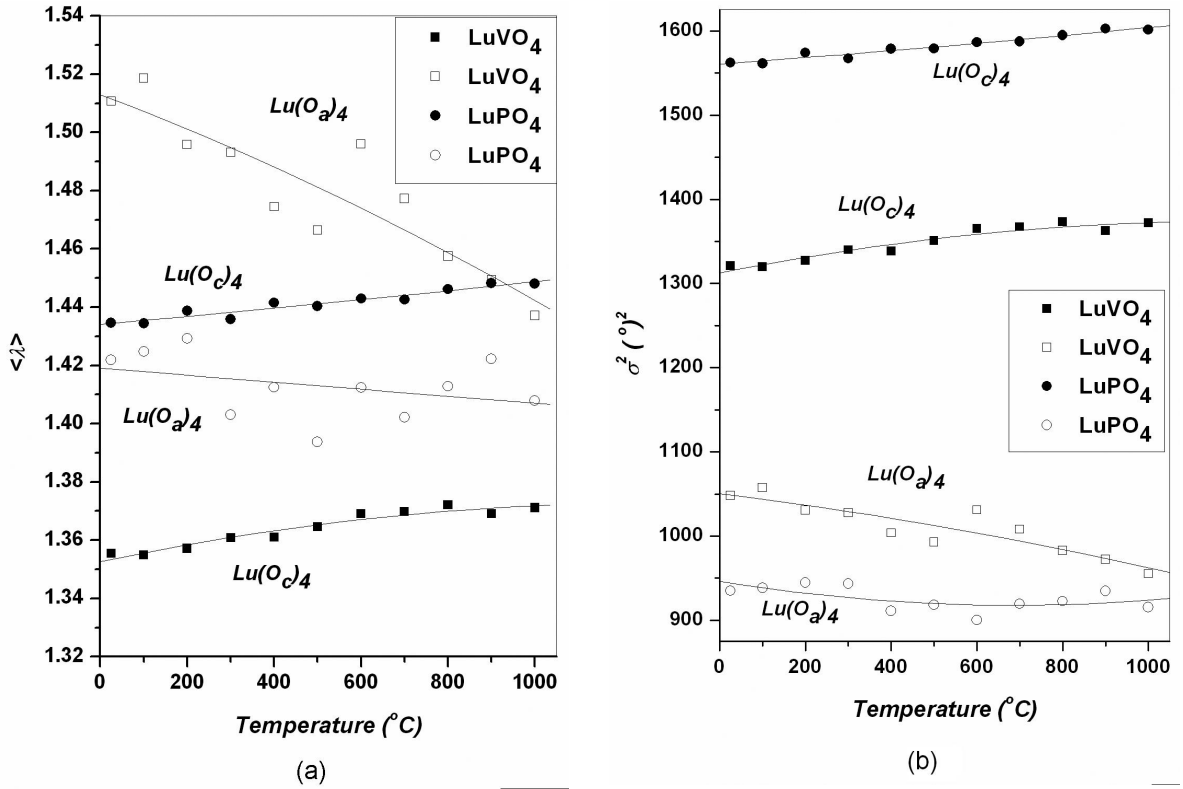

FIGURE 5. Temperature dependence of (**a**) mean quadratic elongation (<λ>) and (**b**) bond angle variances (σ^2) of LuO_4 tetrahedral units in LuO_8 polyhedra.

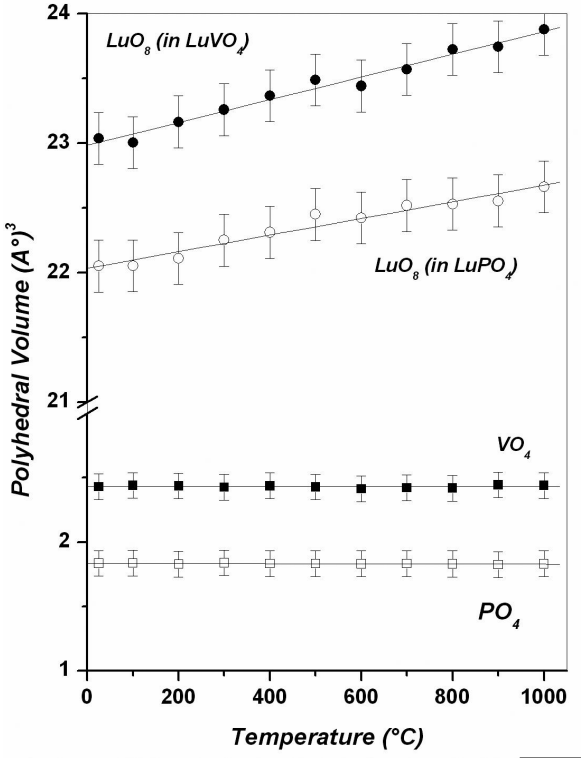

FIGURE 6. Temperature dependence of polyhedral volumes in $LuPO_4$ and $LuVO_4$.

l_0 = bond lengths of corresponding regular polyhedra of equal volume;

θ_0 = regular polyhedral angles.

The variations of <λ>and σ^2 with temperature are shown in Figures 5a and 5b, respectively. The values of <λ> and σ^2 at ambient temperature and 1000 °C for $LuVO_4$ and $LuPO_4$ are given in Table 3. In both the compounds, significant distortions in the $Lu(O_c)_4$ and $Lu(O_a)_4$ are observed. However, the values of <λ> for both tetrahedra in $LuPO_4$ are closer than those in $LuVO_4$. Thus the LuO_8 units in $LuPO_4$ are relatively spherical compared to those in $LuVO_4$. In both $LuPO_4$ and $LuVO_4$, <λ> and σ^2 of $Lu(O_c)_4$ tetrahedra show an increasing trend with temperature, whereas they show a decreasing trend for $Lu(O_a)_4$. The variations of <λ> and σ^2 with temperature for $LuVO_4$ are higher than those for $LuPO_4$.

The differences in the Lu-O bonds in the LuO_8 polyhedra in $LuVO_4$ and $LuPO_4$ correlate to the higher polyhedral volume of the former than the latter. The overall polyhedral volume of the LuO_8 unit in $LuVO_4$ increases significantly with temperature compared to $LuPO_4$ (Fig. 6). The typical polyhedral expansion coefficients of the LuO_8 unit in $LuVO_4$ is about 30% higher than that in the phosphate, yet both compounds have almost identical unit-cell volume expansion. This behavior might arise from the very small expansion along the *a* or *b* axes in $LuVO_4$. Besides, the shorter Lu-O_a bonds have higher single bond-valence(s) and hence show smaller thermal expansion. The variation of the Lu-O_a bonds and the decreasing trend of bond angle variances of the compressed tetrahedra are reflected in the smaller expansion

along the *a* axis. Similar variations of polyhedral volume and the orientation of the bonds along the *a* and *c* axes have been used previously to explain the anisotropic thermal expansion or compressibility of scheelite-type compounds (Achary et al. 2006; Hazen et al. 1985). The high-pressure behaviors of YVO_4 (Wang et al. 2004), $LuVO_4$ (Mittal et al. 2008), and zircon (Hazen and Finger 1979), show a relatively low compressibility along the *c* axis compared to that along *a*- or *b*-axes. Comparison of the thermal expansion and compressibility of zircon-type compounds suggests that the inter-cation interactions along the *c* axis have a possible role in hindering the compressibility and favoring thermal expansion.

ACKNOWLEDGMENT

The authors thank Ian Swainson for his help in editing the text of this manuscript.

REFERENCES CITED

Achary, S.N. and Tyagi, A.K. (2004) Strong anisotropic thermal expansion in cristobalite-type BPO_4. Journal of Solid State Chemistry, 177, 3918–3926.

Achary, S.N., Jayakumar, O.D., Tyagi, A.K., and Kulshreshtha, S.K. (2003) Preparation, phase transition and thermal expansion studies on low-cristobalite type $Al_{1-x}Ga_xPO_4$ (x = 0.0, 0.20, 0.50, 0.80, and 1.00). Journal of Solid State Chemistry, 176, 37–46.

Achary, S.N., Patwe, S.J., Mathews, M.D., and Tyagi, A.K. (2006) High-temperature crystal chemistry and thermal expansion of synthetic powellite ($CaMoO_4$): A high-temperature X-ray diffraction (HT-XRD) study. Journal of Physics and Chemistry of Solids, 67, 774–781.

Aldred, A.T. (1984) Cell volumes of APO_4, AVO_4, and $ANbO_4$ compounds, where A = Sc, Y, La-Lu. Acta Crystallographica, B40, 569–574.

Bayer, G. (1972) Thermal expansion of ABO_4 compounds with zircon and scheelite structures. Journal of Less Common Metals, 26, 255–262.

Beall, G.W., Boatner, L.A., Mullica, D.F., and Milligan, W.O. (1981) The structure of cerium orthophosphate, a synthetic analog of monazite. Journal of Inorganic and Nuclear Chemistry, 43, 101–105.

Boatner, L.A. (2002) Synthesis, structure, and properties of monazite, pretulite, and xenotime. In M.J. Kohn, J. Rakovan, and J.M. Hughes, Eds., Phosphates: Geochemical, Geobiological, and Materials Importance, 48, p. 87–123. Reviews in Mineralogy and Geochemistry, Mineralogical Society of America and the Geochemical Society, Chantilly, Virginia.

Carron, M.K., Mrose, M.E., and Murata, K.J. (1958) Relation of ionic radius to structures of rare-earth phosphates, arsenates, and vanadates. American Mineralogist, 43, 985–989.

Chakoumakos, B.C., Abraham, M.A., and Boatner, L.A. (1994) Crystal structure refinements of zircon type MVO_4 (M = Sc, Y, Ce, Pr, Nd, Tb, Ho, Er, Tm, Yb, Lu). Journal of Solid State Chemistry, 109, 197–202.

Depero, L.E. and Sangalettis, L. (1997) Cation sublattice and coordination polyhedra in ABO_4-type of structures. Jounal of Solid State Chemistry, 129, 82–91.

Errandonea, D., Manjon, F.J., Somayazulu, M., and Housermann, D. (2004) Effect of pressure on the local structure of $CaWO_4$ and $YLiF_4$: Mechanism of the scheelite-to-wolframite and scheelite-to-fergusonite transition. Journal of Solid State Chemistry, 177, 1087–1097.

Evans, J.S.O., Mary, T.A., Vogt, T., Subramanian, M.A., and Sleight, A.W. (1996) Negative thermal expansion in ZrW_2O_8 and HfW_2O_8. Chemistry of Materials, 8, 2809–2823.

Gates, S.D., Colin, J.A., and Lind, C. (2006) Non-hydrolytic sol-gel synthesis, properties, and high-pressure behavior of gallium molybdate. Journal of Materials Chemistry, 16, 4214–4219.

Haines, J., Cambon, O., Cachau-Herreillat, D., Fraysse, G., and Mallassagne, F.E. (2004) Single-crystal X-ray diffraction study of a-quartz-type $Al_{1-x}Ga_xPO_4$. Solid State Sciences, 6, 995–999.

Hazen, R.M. and Finger, L.W. (1979) Crystal structure and compressibility of zircon at high pressure. American Mineralogist, 64, 196–201.

Hazen, R.M. and Prewitt, C.T. (1977) Effect of temperature and pressure on interatomic distances in oxygen based minerals. American Mineralogist, 62, 309–315.

Hazen, R.M., Finger, L.W., and Mariathasan, J.W.E. (1985) High pressure crystal chemistry of scheelite type tungstates and molybdates. Journal of Physics and Chemistry of Solids, 46, 253–263.

Hikishi, Y., Ota, T., Daimon, K., Hattori, T., and Mizuno, M. (1998) Thermal, mechanical, and chemical properties of sintered xenotime-type RPO_4 (R = Y, Er, Yb, and Lu). Journal of American Ceramic Society, 81, 2216–2218.

Jayaraman, A., Batlogg, B., and VanUitert, L.G. (1985) Effect of high pressure on the Raman and electronic absorption spectra of $PbMoO_4$ and $PbWO_4$. Physical Review B, 31, 5423–5427.

Kahle, H.G., Schopper, H.C., Urban, W., and Wiechner, W. (1970) Temperature effects on zircon structure lattice parameters and zero-field resonance for substituted Gd^{3+}. Physica Status Solidi, 38, 815–819.

Kaminskii, A.A. (1990) Laser Crystals, 2nd edition. Springer-Verlag, Berlin.

Khan, A.A. (1976) Computer simulation of thermal expansion of non-cubic crystals: Forsterite, anhydrite, and scheelite. Acta Crystallographica, A32, 11–16.

Knittle, E. and Williams, Q. (1993) High pressure Raman spectroscopy of $ZrSiO_4$: Observation of zircon to scheelite transformation at 300 K. American Mineralogist, 78, 245–252.

Li, H., Zhou, S., and Zhang, S. (2007) The relationship between the thermal expansions and structures of ABO_4 oxides. Journal of Solid State Chemistry, 180, 589–595.

Mittal, R., Garg, A.B., Vijayakumar, V., Chaplot, S.L., Achary, S.N., Tyagi, A.K., Godwal, B.K., Busetto, E., and Lausi, A. (2008) Investigation of the phase stability of $LuVO_4$ at high pressure by powder X-ray diffraction measurements and lattice dynamical calculations. Journal of Physics: Condensed Matter, 20, 075223, 7 p.

Muller, O. and Roy, R. (1974) Crystal Chemistry of Non-Metallic Materials. Vol. 4, The Major Ternary Structural Families. Springer-Verlag, New York.

Mullica, D.A., Sappenfield, E.L., Abraham, M.M., Chakoumakos, B.C., and Boatner, L.A. (1996) Structural investigation of several $LnVO_4$ compounds. Inorganic Chimica Acta, 248, 85–88.

Ni, Y., Hughes, J.M., and Marian, A.N. (1995) Crystal chemistry of monazite and zircon structures. American Mineralogist, 80, 21–26.

Nyman, H. and Hyde, B.G. (1984) Zircon, anhydrite, scheelite and some related structures containing bisdisphenoids. Acta Crystalllographica, B40, 441–447.

Reddy, N.R.S. and Murthy, K.S. (1983) Anomalous thermal expansion of europium vanadate. Journal of the Less Common Metals, 90, L7–L8.

Reddy, N.R., Murthy, K.S., and Rao, K.V.K. (1981) Thermal expansion of dysprosium vanadate. Journal of Materials Science, 16, 1422–1424.

Reddy, C.V.V., Kistaiah, P., and Murthy, K.S. (1985) X-ray studies on the thermal expansion of gadolinium vanadate. Journal of Physics D, Applied Physics, 18, L27–L30.

Reddy, C.V.V., Murthy, K.S., and Kistaiah, P. (1988) X-ray study of the thermal expansion anisotropy in YVO_4 and $YAsO_4$ compounds. Solid State Communications, 67, 545–547.

Reddy, C.V.V., Kistaiah, P., and Murthy, K.S. (1995) X-ray study of the thermal expansion anisotropy in neodymium vanadate. Journal of Alloys and Compounds, 218, L4–L6.

Robinson, K., Gibbs, G.V., and Ribe, P.H. (1971) Quadratic elongation: A quantitative measure of distortion coordination polyhedra. Science, 172, 567–570.

Rodriguez-Caravajal, J. (1990) FULLPROF: A Program for Rietveld Refinement and Pattern Matching Analysis. Satellite Meeting on Powder Diffraction, XV International Union of Crystallography Congress, 127, Toulouse, France.

Schopper, H.C., Urban, W., and Ebel, H. (1972) Measurements of the temperature dependence of lattice parameters of some rare earth compounds with zircon structure. Solid State Communication, 11, 955–958.

Scott, H.P., Williams, Q., and Knittle, E. (2002) Ultra low compressibility silicate without highly-coordinated silicon. Physical Review Letters, 88, 015506, 4 p.

Sen, A., Chaplot, S.L., and Mittal, R. (2003) Molecular dynamics simulation of pressure-induced phase transitions in $LiYF_4$ and $LiYbF_4$. Physical Review B, 68, 134105, 8 p.

Skanthakumar, S., Loong, C.-K., Soderholm, L., Nipko, J., Richardson Jr., J.W., Abraham, M.M., and Boatner, L.A. (1995) Anomalous temperature dependence of the lattice parameters in $HoPO_4$ and $HoVO_4$: Rare earth quadrupolar effects. Journal of Alloys and Compounds, 225, 595–598.

Subbarao, E.C., Agrawal, D.K., McKinstry, H.A., Sallese, C.W., and Roy, R. (1990) Thermal expansion of compounds of zircon structure. Journal of American Ceramic Society, 73, 1246–1262.

Taylor, D. (1986) Thermal expansion data. X. Complex oxides ABO_4. Journal of the British Ceramic Society, 85, 147–155.

Varga, T., Wilkinson, A.P., Lind, C., Bassett, W.A., and Zha, C.-S. (2005) High-pressure synchrotron X-ray powder diffraction study of $Sc_2Mo_3O_{12}$ and $Al_2W_3O_{12}$. Journal of Physics: Condensed Matter, 17, 4271–4283.

Wang, X., Loa, I., Syassen, K., Hanfland, M., and Ferrand, B. (2004) Structural properties of the zircon- and scheelite type phases of YVO_4 at high pressure. Physical Review, B70, 064109, 6 p.

Zhao, S., Zhang, H., Wang, J., Kong, H., Cheng, X., Liu, J., Li, J., Lin, Y., Hu, X., Xu, X., Wang, X., Shao, Z., and Jiang, M. (2004) Growth and characterization of the new laser crystal Nd:$LuVO_4$. Optical Materials, 26, 319–325.

MANUSCRIPT RECEIVED DECEMBER 18, 2007
MANUSCRIPT ACCEPTED JUNE 30, 2008
MANUSCRIPT HANDLED BY IAN SWAINSON